Preliminary results of the modeling of air quality at neighborhood scales

Jason Ching[1*], Tanya L. Otte[1], Sylvain Dupont[1], and Avraham Lacser[2]

[1]Atmospheric Sciences Modeling Division, NOAA ARL, Research Triangle Park, North Carolina (On assignment to the National Exposure Research Laboratory, U.S. EPA)

[2]Israel Institute for Biological Research, Ness Ziona, Israel

**Corresponding author address*: Jason Ching, AMD/NERL/USEPA, MD D243-03, Research Triangle Park, NC 27711; e-mail: ching.jason@epa.gov

Abstract

Air quality (AQ) simulation models provide a basis for implementing the National Ambient Air Quality Standards (NAAQS) and are tools for performing risk-based assessments for air toxics and for developing and testing environmental management strategies. Our conceptual design basis for air quality models to be used in estimating human exposure to pollution, especially in the geographic context of urban population centers, will requires both grid modeling at neighborhood scales (NS) and an estimate of sub-grid-scale variability in the pollutant concentration fields at each grid and for each model time. To address the first requirement, an urban canopy parameterization (UCP) is implemented inside the U.S. EPA Models-3 Community Multiscale Air Quality (CMAQ) through the Penn State/NCAR Mesoscale Model (MM5) which provides meteorological fields to CMAQ. This UCP is based on the drag-force approach to simulate meteorological fields inside the urban roughness sub-layer. This modeling approach is meant to enhance and complement the more limited data from monitoring networks to provide the concentration fields at high temporal and spatial resolutions.

The impact of this UCP on meteorological and pollutant fields is studied for a simulation centered in the Philadelphia urban area. It is shown that the meteorology fields and the subsequent AQ fields are both sensitive to the UCP; its implementation produces significantly different results at neighborhood scales. In future work, the design requirement for linking ambient concentration modeling to estimate human exposure will involve introducing estimates of variability at sub-grid scales. That requirement and initial methodology are also briefly discussed.

I INTRODUCTION

Air quality (AQ) simulation models provide a basis for implementing the National Ambient Air Quality Standards (NAAQS) and are tools for performing risk-based assessments and for developing environmental management strategies. In this study, we discuss specific requirements for AQ models to provide the concentration information to drive human exposure models such as the Stochastic Human Exposure to Dose System (SHEDS) (Burke et al. 2001). Since population and their human activity is concentrated in urban areas, the exposure context requires modeling for areas in which emissions and subsequent air quality distributions are strongly influenced by the presence of urban morphological structures (UMS)of varying complexities. Grid models provide the means for determining the spatial and temporal distribution of air quality from local and regional sources. Reducing the model grid size makes possible the modeling of spatial gradients in pollutant concentration fields arising from dispersion and photochemistry of large source emissions. The grid size controls the extent to which the spatial fields are resolved. Inherent spatial details at smaller than model grid sizes may be very large near sources, as a result, near-source peak-to-grid mean concentrations may be large. Thus, both the grid and sub grid concentration are needed for assessing exposure. Indeed, our conceptual framework for risk assessment and exposure modeling is composed of two major modeling elements: i) modeling at high spatial resolution grid, and ii) modeling the sub-grid concentration distributions. These two elements and monitoring data complete the information needed for risk assessment and exposure modeling.

Both measures are impacted by the impacted by the flow and dispersion fields which are strongly influenced by the presence of urban morphological structures. It is well known that meteorological fields have a profound impact on the AQ simulation (cf., Pielke and Uliasz 1998, Seaman 2000). As we require smaller grid resolutions to provide air quality simulations at neighborhood scales in urban areas suitable for driving exposure models, the more important it becomes for developing and implementing appropriate parametric formulations that can represent the effect of urban structures on the dynamics and thermodynamics of the meteorological fields within and above the urban roughness sub layer (RSL). An ability to accurately describe such flows will improve the accuracy of the air quality predictions resulting from sources located within urban canopies. Above the canopy, these UMSs will also strongly influence the meteorology structure and the subsequent predictions of urban to regional scale air quality.

Given the need to model air quality at grid sizes commensurate with the spatial gradient of

concentration gradients in urban areas, and recognizing that even at small grid sizes, subgrid variations may exist that impacts exposure, it is the objective of this study to address their technical issues, and to perform experiments to elucidate their requirements. However, while it is important to address both resolved and sub-grid modeling, the scope and complexity on resolved scale modeling preclude a full examination of both. Thus, this paper will focus primarily on grid resolved scale modeling. The methodologies associated with deriving estimates of SGV will be subject of a complimentary paper, but a brief discussion will be provided at the end of this paper in the section "Future directions".

For this study the U.S. EPA Models-3 Community Multiscale Air Quality (CMAQ) modeling system (Byun and Ching 1999) is used. The meteorological fields are provided by the Penn State/NCAR Mesoscale Model (MM5). The methodology that we adopt to simulate with Models-3 at high resolution is to modify the Gayno-Seaman planetary boundary layer (GSPBL) scheme of MM5 to incorporate an urban canopy parameterization (UCP) based on the drag-force approach (DA) which can provide meteorological fields inside the RSL. For our study, a model domain and study area centered on the Philadelphia Metropolitan area was set up and the CMAQ model was run for simulations at horizontal grid dimensions of 36 km, 12 km, 4 km, and 1.33 km, the latter representing the neighborhood scale resolution with an additional number of vertical layers inside the urban canopy to incorporate UCP. Being the first time that Models-3 is used at NS, it is shown that the current version of the GSPBL scheme is not satisfactory for unstable condition, the implementation of the turbulent length scale parameterization of Bougeault & Lacarrère (1989), hereinafter BL89, gives better results. Preliminary results will be presented and discussed to illustrate the impact of introducing UCP for modeling at NS on meteorological and pollutant fields.
In section II, the approach used to simulate AQ at high spatial resolution with CMAQ is presented with the description of the UCP implemented inside MM5. Section III describes simulation configurations for MM5, emission and chemistry for the Philadelphia case. The resulting modeled meteorological and air quality fields are presented in section IV, and a summary of findings from these first simulations at NS with CMAQ are presented in section V. Finally, in section VI, a description and discussion of the future directions to complete the framework to assess AQ at NS with a focus on the UCP refinements and a brief discussion regarding aspects of sub-grid concentration distribution modeling.

II. APPROACH TO SIMULATE AT HIGH RESOLUTION

The meteorological fields at NS result from the interactions between the larger-scale meteorology and the manner in which urban morphological structures characteristics of the urban canopy affect their dynamics and thermodynamics. Since there is significant heterogeneity in the urban canopy, the meteorological fields in the urban canopy can be very complex. Given the current computer capacity, it may be impractical for operational purposes, to use sufficiently fine grid spacing in the model to explicitly simulate the flows around the individual surface obstacles (e.g., buildings and trees) for an entire city and surrounding area. For such applications, CFD and other very fine scale modeling can provide such details. Typically, the aerodynamic characteristics of the urban surface are represented as highly simplified parameterizations in the mesoscale models. Such models typically apply the roughness approach (RA), where the influence of surface obstacles is represented by gridded roughness length and a displacement height; the dynamics and thermodynamics surface exchange coefficients are calculated from the Monin-Obukhov (MO) similarity theory. However MO theory assumes stationary conditions and spatial homogeneity, and these assumptions break down in the urban RSL. Furthermore, the RA cannot simulate the thermodynamic profiles below the displacement height and does not reproduce the turbulent kinetic energy maximum observed above the urban canopy (Rotach 1995). The RA does not define the RSL structure, and it cannot distinguish pollutant sources inside the urban canopy from those located at the roof level. Thus, the RA may be inappropriate for simulating AQ at NS in urban areas.

To improve the mesoscale model simulation of meteorological fields inside the urban RSL, the DA, initially used for the vegetation canopy (Yamada 1982), has been recently extended to the urban canopy (cf. Brown and Williams (1998) and Martilli et al. (2002)). In comparison to the RA, the lower level of the computational domain in the DA corresponds to the real level of the ground (no displacement height), and some vertical layers are within the urban canopy to allow more detailed meteorological fields in the urban RSL (see Figure 1). For this study, an UCP was introduced into the Fifth-Generation Pennsylvania State University/National Center for Atmospheric Research Mesoscale Model (MM5; Grell et al., 1994) following the DA described by Brown and Williams (1998) and Brown (2000). Inside the urban canopy, the grid-cell-averaged effect of the building structures on the dynamics and thermodynamics is parameterized following the local characteristics of the urban morphology. This UCP requires the canopy area density within each grid cell, as well as a distribution of anthropogenic heat generated from each grid cell. Figure 1 illustrates some of the localized impacts to the urban meteorology that are captured in the UCP.

In the UCP, the dynamic effects of buildings are represented by adding a frictional force

created by these buildings in the momentum equations, and a source term in the turbulence kinetic energy equation, depending on the canopy area density. In our implementation of the UCP in MM5, we use the DA to represent the dynamic effects of buildings; the representation of the dynamic effects of the vegetation and bare soil especially outside the urban area uses the RA in this version of the UCP. It is important to note that the RA is here applied with a thinner first vertical layer than in a typical application of MM5, and this reaches the theoretical limit for the RA. In the UCP, it is assumed that the buildings affect the flow, virtually, because of their vertical and horizontal surfaces but they do not take up any volume within the grid cell. The UCP modifications to the momentum and TKE equations were implemented in the GSPBL scheme (e.g., Shafran et al., 2000).

Modifications to the thermodynamics for this UCP consider three urban impacts to the energy budget. First, a time-varying anthropogenic heat flux (e.g., Taha 1999) was introduced into the heat equation (e.g., Chin et al., 2000). The maximum anthropogenic heat flux is set following Pielke (1984). The heat equation also includes the heat contribution to the city canyons following Yamada (1982); the contribution due to rooftops has not yet been implemented. The surface energy balance includes the shadowing/trapping effect of the net radiation reaching the ground in the city canyons modified by the extinction of the radiation through the urban canopy using a simple exponential function (e.g., Brown 2000). These changes were implemented in MM5 in the "slab" surface model (Zhang and Anthes, 1982), the Rapid Radiative Transfer Model (Mlawer et al., 1997), and in the temperature tendency equation.

More specific information on the implementation of the UCP in MM5 can be found in Otte and Lacser (2001, 2002), Lacser and Otte (2002), and in a forthcoming article.

III. SPECIFICATIONS FOR THE SIMULATION

Our study focuses on simulating the meteorology and chemistry at NS for Philadelphia, Pennsylvania, on 14 July 1995. This study day is characterized by high pressure, abundant sunshine, abnormally high temperatures, and largely stagnant conditions on the eastern United States and southern Canada, which were favorable for the progressive production of ozone and transport of precursor pollutants. Additional discussion of the meteorology and chemistry of this case can be found in Berman et al. (1999) and Seaman and Michelson (2000). In this section, the configurations used for the meteorology (a), the emissions (b) and the chemistry (c) are described.

a. Meteorology configuration

MM5 Version 3 Release 5 was run in a one-way nested configuration for several days in July 1995. The five nested MM5 computational domains included 108, 36, 12, 4, and 1.33 km horizontal

grid spacing. Figure 2 shows the location of the 4-km and 1.33-km computational domains focused on Philadelphia, Pennsylvania. Since the UCP was exclusively used in the 1.33-km domain, the majority of the model description will focus on that domain. The first four domains were run with 30 vertical layers (about 12 layers in the PBL, and lowest layer depth of 38 m) and physics options appropriate for each resolution. Four-dimensional data assimilation (FDDA) was used as a dynamic analysis on those four domains following Stauffer and Seaman (1994). The 1.33-km domain includes 112 x 112 grid points covering the Philadelphia metropolitan area. The 1.33-km domain was run in MM5 with the following user options: the GSPBL scheme (Shafran et al., 2000), force-restore "slab" soil model (Zhang and Anthes 1982), the Rapid-Radiative Transfer Model (Mlawer et al., 1997) for long-wave radiation, Dudhia short-wave radiation (Dudhia 1989), mixed-phase microphysics (Reisner et al., 1998), and explicit convection. FDDA was not used in the 1.33-km domain so that the influence of the UCP could be evaluated independently. The 1.33-km domain was initialized at 00 UTC 14 July 1995 with an interpolated initial state and lateral boundary conditions based on the simulation on the 4 km domain. All simulations with the 1.33-km domain cover 24-h periods ending 00 UTC 15 July 1995. Simulations with the RA in the 1.33-km domain used the 30-layer vertical structure. To include the influence of smaller obstacles, the UCP was used on the 1.33-km domain with 40 layers that included ten new layers in the lowest 100 m (lowest layer depth of 4 m). Above 175-m AGL, the layer structures are identical.

In most applications of MM5 (using the RA), the urban areas are generally assumed to be homogeneous (based on land use), and characterized with the same physical attributes such as roughness length, moisture availability, and albedo. For our UCP application, we have added an urban category overlay to the MM5 land use classification; ideally, a true (commercially available) morphological data base would be used in this type of application. The characterization of the urban morphology in this application loosely follows Ellefsen (1990–91) who defines 17 urban terrain zones that represent age, intended use, construction, and density of buildings within the urban area. For this study, Ellefsen's urban terrain zones were aggregated to six categories (modified based on Grimmond and Oke 1999) to represent urban categories such as high-rise, industrial, and urban residential. A seventh category was added to cover urban areas within the modeling domain but outside of Ellefsen's study, and that category is generally assumed to be a lower-density urban area (e.g., suburban). Each of the seven urban subcategories has a different value for morphological variables that are used in the UCP. The maximum building height and canyon fraction within the urban area are defined following Ellefsen (1990–91). The canopy area density is defined in each grid cell in our application from a linear function that relates the maximum height of buildings and the building plan area fraction in the grid column. The soil moisture is set from summer climatological values as a function of dominant land-use category (Grell et al., 1994).

b. Emissions Configuration

The emissions were processed using the Sparse Matrix Operator Kernel Emissions (SMOKE) Modeling System, Version 1.3 (Houyoux et al., 2000). Within the continental U.S., the U.S. EPA National Emissions Trends Inventory, Version 3.11, for 1996 was used for area, point, and mobile sources of emissions. The 1995 emissions data were "regrown" back from the 1996 database. The county-based mobile source data were reallocated to the highways to accommodate the need for accurate apportionment to the various grid resolutions used in the study. Area- and point-source emissions for Canada were represented from a database for 1985 (Saeger et al., 1989) that was "grown" incrementally to 1990 and 1995. Data for mobile sources in Canada were obtained directly from the U.S. EPA Office of Air Quality Planning and Standards. Biogenic emissions were computed for all land-based geographical areas using the second version of the Biogenic Emissions Inventory System (BEIS2) (Pierce et al., 1998) which estimates volatile organic compound (VOC) emissions from vegetation and nitric oxide (NO) emissions from soils.

In most applications of SMOKE, the near-surface sources of emissions (area, mobile, and biogenic) are typically applied into the lowest model layer which is generally above the urban canopy and 38 m thick in this application. However for the UCP application, there are several model layers within the urban canopy. For the UCP application, the near-surface emissions were spread into an equivalent model depth of the lowest layer of the non–UCP application, or the lowest eight model layers (up to 37 m above the surface). The emission spreading was mass-weighted so the deeper layers in the urban canopy would acquire a greater percentage of the near-surface emissions. For example, the layer closest to the surface (4 m thick) received 10.4% of the near-surface emissions, while the eighth layer from the surface (6 m thick) received 16.7% of the near-surface emissions.

c. Chemistry Configuration

The chemistry was run for this case using the U.S. EPA's Community Multiscale Air Quality (CMAQ) Modeling System (Byun and Ching 1999) release for June 2002. For these experiments, CMAQ's version of the fourth carbon-bond chemical mechanism (CB4) (Gery et al., 1989) was used. CB4 considers nine primary organic species that are generally of the carbon–carbon bond types. Ethene, isoprene, and formaldehyde (with similar chemical bonds) are represented explicitly while other organic compounds are assigned to a species group based on molecular structure. Aerosol reactions were added to CB4 following Binkowski and Shankar (1995). The chemistry was solved using the Euler backward iterative method described by Hertel et al. (1993) and modified for CMAQ following Huang and Chang (2001). The horizontal advection was calculated using the piecewise parabolic method (Colella and Woodward 1984), and multi-scale horizontal diffusion was used. Dry deposition velocities were calculated for sixteen gaseous species following Wesely (1989).

The effects of sub-grid clouds on the aqueous chemistry were included in domains with horizontal grid spacing of 12 km or larger; clouds were explicitly resolved in domains with smaller horizontal grid spacing. In addition, CMAQ was modified to compute the eddy diffusivity field based on the algorithms in the GSPBL scheme so that the influences of the TKE could be captured for that field to be more consistent with the MM5 simulations.

CMAQ was run for four domains (36, 12, 4, and 1.33 km horizontal grid spacing) for a period preceding and including the day of interest, 14 July 1995. The CMAQ computational domains were based on the MM5 domains of the same grid spacing. The outermost six or seven grid cells on the lateral boundaries from each MM5 domain were not used in CMAQ so that the boundary effects from the meteorological model would be minimized in CMAQ. Runs for the 36-km regional domain was initialized with "clean chemistry" starting at 00 UTC on 7 July 1995, and it was allowed several days to spin-up the chemical background. Accordingly, the 12-km domain was initialized at 00 UTC 11 July 1995 with chemistry from the 36-km domain. The 4-km domain was initialized at 00 UTC 11 July 1995 from the 12-km domain, and the 1.33-km domains were initialized at 00 UTC 14 July 1995 from the 4-km domain.

The vertical structure of the CMAQ domains was based on the vertical structure used in the MM5 simulations. For the simulations on the 36-km, 12-km, and 4-km domains, a 21-layer vertical structure was designated from the 30-layer MM5 configuration. In the 21-layer CMAQ runs, the lowest twelve layers (i.e., up to approximately 1300 m above the surface) are identical to the MM5 vertical structure. The remaining nine layers of that structure each represent the total thickness of two MM5 layers combined to the top of the atmosphere (taken to be 100 hPa in this case). This layer configuration tends to preserve the structure of the PBL as simulated by MM5, and it aims to minimize the effects of vertical interpolation where pollutant emissions and transport are likely to be most important for NS applications. The 1.33-km simulation that was based on MM5 input with the roughness approach (i.e., without the UCP) also used the 21-layer configuration in CMAQ (as that configuration had 30 layers in MM5). The 1.33-km CMAQ simulation that was based on MM5 input with the drag approach (i.e., with the UCP) contained 31 layers. In the 31-layer CMAQ run at 1.33-km, the lowest 22 layers (i.e., up to approximately 1300 m above the surface) were identical to the MM5 vertical structure. The remaining nine layers are defined for the 31-layer structure as in the 21-layer structure.

IV. RESULTS

In this section, the impact of the UCP implementation on meteorological (a) and pollutant (b) fields is presented with also a focus on the effects of the turbulent length scale modification and

of the high resolution of pollutant concentration.

a. Meteorology

Several simulations were made with the 1.33-km domain to determine the impact of the UCP on the MM5 simulation. Since we are primarily interested in CMAQ's ability to simulate the AQ at NS, the evaluation of MM5 focuses on fields that affect the pollutant transport near the surface. Here we only show results from two MM5 simulations: a 30-layer simulation that used the RA (hereafter, *nocan*), and a 40-layer simulation with the UCP (hereafter, *can*). The objectives of this section are to show that MM5 with the RA is not able to correctly simulate the dynamic and thermodynamic fields at NS, and that the modifications to the turbulent scheme and the introduction of the UCP in MM5 improve the simulation of the meteorological fields inside the RSL. Comparisons are made between the *nocan* and *can* cases on a horizontal cross-section located above the urban canopy and on vertical profiles located at the city center (see Figure 2). These comparisons show the impact of the UCP on the turbulent structures of the urban RSL, where pollutants are emitted, and on the mixing height (MH), the effective volume in which the pollutants are dispersed. The UCP used in this study will be the subject of a stronger validation of the dynamics and thermodynamics fields in a forthcoming article.

i. Modifications to the Gayno-Seaman PBL model

Initial simulations with the 1.33-km domain (both with and without the UCP) showed a tendency to generate undulations in the physical fields similar to horizontal convective rolls (e.g., Brown 1970) but with some numerical complications. These undulations are oriented approximately parallel to the mean wind, and they appear during convective conditions in the MH, wind, and temperature fields. The undulations increase in intensity and amplitude throughout the day and are at their maximum amplitude in the late afternoon prior to sundown (approximately 6 p.m. LDT). Figure 3a presents the MH and wind vectors simulated by MM5 at 6 p.m. (LDT) on a horizontal cross-section 55 m AGL using the initial GSPBL. These oscillations show changes in MH of nearly 1 km or more throughout the domain over horizontal distances of less than 10 m. Although horizontal convective rolls have been observed in other studies of urban environments (e.g., Kropfli and Kohn 1978), they are too strong here to be realistic. This problem has commonly been observed by other mesoscale modelers who decrease their horizontal grid spacing to the order of 1 km (D. Stauffer, personal communication, 2002).

A comparison with the Asymmetrical Convective Model (ACM) of Pleim and Chang (1992) for the same case (not shown), using a non-local closure scheme, has shown that the MH assessed with the GSPBL model is underestimated. This result suggests that the numerical undulations with the GSPBL can be explained by insufficient turbulent mixing inside the PBL. Other research (cf.

Zhang et al., 2001) noted that GSPBL tends to underestimate the turbulent mixing and as well as the MH. Bélair et al. (1999) also suggested that local closure schemes (like the GSPBL) tend to underestimate mixing inside the PBL during convective conditions. To solve this problem, the parameterization of the turbulent length scale of Bougeault and Lacarrère (1989) (hereafter, BL89), including a non-local feature in K-coefficient turbulence schemes, has been implemented inside GSPBL only for convective conditions. The new mixing length in GSPBL (following BL89) is derived from the potential upward and downward displacements that could be achieved by parcels having kinetic energy equal to the mean TKE before being stopped by buoyancy effects. Figure 3b presents the same plot as Figure 3a but with the modified GSPBL following BL89. There is no signal of the undulations as in Figure 3a, and the wind field above the canopy is smooth. In addition, the MH in Figure 3b is now slightly higher than that in Figure 3a because the increase of the turbulent length scale increased the mixing inside the PBL. This MH increase is only seen during the day when BL89 is used. We can also see on Figure 3b that the urban area induces a higher MH above and downwind of the urban core due to stronger convection cells induced by the warmer urban surfaces.

ii. Impact of the UCP

Figure 4 compares the turbulent structures inside the urban RSL simulated for the *nocan* and *can* cases for a column above a grid cell at the city center. In Figures 4a and 4b, the vertical profiles of frictional velocity (u_*) and TKE at 2 p.m. (EDT) are plotted against normalized height (z/h) where h is the average building height. Figures 4a and 4b are similar to figures 4 and 12 of Martilli et al. (2002) (hereafter, M02) to facilitate the comparison with those results. For the *nocan* case, the u_* profiles are constant in the RSL which is consistent with the constant flux layer theory used by the RA. In the *can* case, u_* has a weak maximum around $z/h \sim 2$ and decreases inside the canopy. Contrary to the *nocan* case, the TKE profile for the *can* case reaches a maximum inside the canopy at the mean level of building roofs ($z/h = 1$) before decreasing near the ground.

M02 and Vu et al. (2002) have observed with their UCPs the same behavior of the normalized u_* profile as with the UCP in MM5 shown in Figures 4a and 4b. Our UCP profiles are very similar to the profiles in M02 at the RSL level, which fit well with measurements of Rotach (2001). Figure 4a shows a subtle u_* maximum at z/h 2.2 for the *can* case, and a gradual decrease of u_* toward the surface. Measurements of Feigenwinter et al. (1999) and Oikawa and Meng (1995) above an urban canopy show also a maximum of u_* at $z/h = 2.1$ and $z/h = 1.5$, respectively, before decreasing slowly with the height, but this maximum was not observed by Feigenwinter et al. (1999) under unstable conditions. Figure 4b shows a maximum of TKE at z/h 1 for the *can* case, with a rapid decrease of TKE toward the surface. M02 obtained a maximum TKE profile inside the canopy only during the night, and Vu et al. (2002) obtained a maximum at the mean roof level

except under strong unstable conditions. Measurements shown by M02 seem to be very variable, and it is not clear if the TKE reaches a maximum inside the canopy during unstable conditions. Kastner-Klein et al. (2000) observed in three different wind tunnels a maximum of TKE at $z/h \sim 1.4$ above a street canyon for neutral stratification. Measurements of Christen et al. (2002) in Basel, Switzerland, had also a monthly average profile of maximum TKE at $z/h \sim 1$.

Figure 4c presents the vertical profile of the potential temperature for the *can* and *nocan* cases at 6 a.m. (LDT). It shows that using the UCP in the *can* case creates a neutral layer up to 200 m AGL during the night, whereas in the *nocan* case the lower atmosphere is clearly stable. The profile of potential temperature in the *can* case is consistent with the reduction of the atmosphere stability near urban surfaces (Roth 2000). As in M02, the depth of the neutral layer is in agreement with the values given by Oke (1995).

Figure 5 shows the differences between the *can* and *nocan* cases (*can* minus *nocan*) on the MH (left panel), and the wind vectors and air temperature (right panel) at 55 m AGL throughout the day. At 6 a.m. (Figure 5a), the air temperature above the urban canopy and downwind of the city is up to 4 K warmer in the *can* case which induces a higher MH (greater than 250 m difference in the urban core). Figure 5a shows a clear reduction in the magnitude of the southwesterly winds in the urban core with UCP, as is expected. Since the DA used in the *can* case decreases the wind velocity above the urban canopy, at 55 m the flow seems to skirt around the city more than with the RA. The meteorological fields above rural areas are very similar in the two cases at this time. At 2 p.m. (Figure 5b), the difference in air temperature between both cases is small (<1 K). At that time, the air is slightly warmer downwind of the city in *can* case. The difference in wind speed is very small because convective developments at this time of the day attenuate the influence of dynamic fields. It appears that the local differences of the MH in Figure 5b are related to the local differences of the air temperature, particularly downwind of the city. At 6 p.m. (Figure 5c), the air temperature and MH above the city is slightly higher in the *can* case, whereas around the city (lateral side) they are smaller which can be explained by the stronger flow around the city.

b. CMAQ Simulation Results

In this section, we explore the sensitivity of CMAQ to the turbulent length scale modification inside GSPBL scheme and to the UCP incorporated into the MM5 at the fine scale resolution. For the UCP sensitivity, surface pollutant fields and pollutant vertical profiles at the center of Philadelphia are compared with (hereafter, *can*) and without UCP (hereafter, *nocan*). Subsequently, the characteristics of the surface modeled concentration fields at the four different grid resolutions, 36 km, 12 km 4 km and 1.33 km are presented to show the local variability of pollutant concentration. Results are shown for CO, a relatively slow reacting pollutant, and ozone

and NO which are more photochemically active, and for two aldehydes which are photochemically active hazardous air toxic pollutants.

i. Sensitivity of pollutant fields to BL89 at the neighborhood scale without UCP

As seen on meteorological fields, the standard version of GSPBL scheme induces numerical undulations that have been removed by using BL89. These numerical undulations are also manifested in the air quality fields as seen in Figure 6a. This figure compares the modeling differences between run made with BL89 from that for which BL89 but normalized by the run made with BL89. The undulations in the simulation reveal an evolution with time, and during this day, they seem to be the most pronounced at 2pm EDT. Note that the same scale applies to each of the the four pollutants depicted. As a fractional difference the character of the undulations do exhibit subtle differences between the pollutants shown in the figure. Figure 6b presents the difference of CO surface fields at 6 p.m. (LDT) with and without BL89 normalized by the BL89 results. Here the undulation for the CO appears to be less pronounced, since the maximum heat flux that cause these spurious wave-like features has diminished from its daytime maximum. We note in this figure, however, that the as anticipated, implementation of BL89 causes the modeled CO concentration to be lower by more than 50% in the urban area because of the increase of the MH with BL89 observed in the section 4a. A modification of 250 m of the MH can thus induced a large change on pollutant concentration.

ii. Sensitivity of pollutant fields to the UCP at the neighborhood scale

Figure 7 presents the difference of CO surface fields at 6 p.m. (LDT) between the *can* and *nocan* cases normalized by the *can* case results. In the section 4b, it has been observed that the predicted MH over the urban area is larger at the end of the day and during the night with the UCP than without. This induces, now, a lower concentration of CO due to the enhanced dilution. For this simulation, the normalized difference is in excess of 50% or more over the urban area. As in Figure 7, the Figure 8 shows the influence of the UCP on photochemical pollutant surface fields, NO_x (Figure 8a) and ozone (Figure 8b). The results show significant impact of the UCP on the predicted fields; the magnitude of positive and negative differences in the NO_x distributions exceeded 150%. As a consequence, the resulting ozone also displayed large differences varying by about a factor of two.

To see the influence of the UCP on the vertical structure of pollutant fields, their vertical profiles are shown in Figure 9 for the same point used in Figure 3 for a central site in downtown Philadelphia, for early afternoon period (2 p.m. LDT). For meteorological fields, we have observed in section 4a that the impact of the UCP is stronger inside and just above the urban canopy with a maximum of TKE at the roof level and a decrease of u_* inside the canopy. For pollutant fields, it

seems that the UCP increase the mixing in the lower level of the atmosphere (< 800 m) with a vertical gradient for O_3, NO and NO_x near zero up to 400 m whereas on the *nocan* case profiles seem to increase linearly for O_3 and decrease linearly for NO and NO_2 from the ground. For the two aldehydes the vertical profiles are slightly similar for both case. As observed in section 4a, at this time of the day, the difference of MH between *can* and *nocan* case is the smallest, thus the increase of mixing in the lower part of the atmosphere can be attributed to the increased turbulence inside the RSL induced by the UCP. Note that for the *can* case the surface ozone value is higher whereas the surface NO and NO_2 values are lower. For the *nocan* case, the surface ozone was nearly all titrated consistent with its NO distribution. On these profiles, no discontinuity due to the urban canopy has been seen, whereas, we could expect that the pollutant dilution inside the canopy is smaller than just above the canopy inducing a stronger concentration of small reactive pollutant inside the canopy. The turbulent length scale parameterization is the same inside and above the canopy whereas turbulent structures are broken in contact to the urban canopy elements that should be considered as proposed by Martilli et al. (2002). It is depend also on the emission distribution inside the canopy.

iii. Sensitivity of pollutant concentration to the grid resolution

The four panels shown on Figure 10 are the modeled CO at the four different grid resolutions, 36 km (a), 12 km (b), 4 km (c), and 1.33 km (d). Clearly, the fine grid mesh predictions depict fine scale features in the spatial distribution. The patterns of high CO are clearly seen to be associated with the major traffic corridors extending southwest to northeast through Philadelphia. For this simulation, the vehicle miles traveled, (VMT) data that is typically apportioned on a county basis, but which was reapportioned to the highway system for this study provided the ability for fine scale features observed in the NS runs to be revealed. These features clearly become less resolved as the grid size increases. Moreover, the magnitudes of the peak values are seen to increase roughly inversely with the grid size because the average is in a smaller volume. In this case, the range of maxima over central Philadelphia ranged from <0.4 ppmV @ 36 km resolution to values in excess of 1.2 ppmV at 1.33 km. Also, the predictions at 1.33 km reveal complex structures in the spatial gradients. This also indicates large spatial variability in the magnitude of the gradient distributions. Also (not shown), the time series of the CO show an increase in the range of the magnitude of the peak (0.5. 0.8, 1.2 to 2.0 ppbV) with decreasing grid mesh size from 36 to 1.33 km respectively.

The four panels format of Figures 11 and 12 depict the multi-grid resolution simulation for NO_x and ozone respectively as in the previous figure for CO. It can be seen that the results are qualitatively similar to that of CO in terms of the relatively greater resolving power of the fine scale spatial features when modeling with small grid sizes. However, in addition to enhancing the spatial distribution of the pollutants, the added spatial resolution of the modeled NO_x concentrations at NS

due to reapportionment of county based VMT data to highways in the emissions model also impacted the spatial distribution of the ozone concentration distribution. As an important precursor of ozone, the NO_x and ozone distribution should be correlated. However, since NO_x from mobile sources is typically emitted initially as mostly NO, this causes the ozone in proximity to be titrated resulting in an initial rapid depressing of the ozone concentration. As clearly seen, the results depict considerable differences in the characteristics of the spatial distribution of NO_x with grid size. As a result, the added resolution of the NO_x fields greatly affects the resulting ozone distributions. The smaller grids sizes begin to resolve the titration effect of NO on ozone showing regions of markedly lower ozone in the enhanced NO_x areas, especially along the major traffic corridors. As a result, both the characteristics of the spatial distribution as well as the ozone magnitude are considerably dependent on the grid mesh size. It is well known that the grid mesh size plays an important role in regional to urban scale photochemical modeling (Ku et al., 2001). The results when modeling at NS provides much increased levels of detail and complexities to the spatial structure for photochemically active pollutants.

For air toxic, many such pollutants can be expected to exhibit high concentration or "hot spots". Figure 13 shows examples depicting hot spot areas for formaldehyde and acetaldehyde within the major urbanized area of metropolitan Philadelphia. These hot spots are primarily associated with industrial sources, but high values are also exhibited along the major traffic corridors. These fields are, of course, results from a combination of dispersion of primary sources as well as from photochemistry. We noted that simulation at larger grid size did reduce the magnitude of the concentration "hot spots"; consequently, this would reduce the predicted risk impacts. Further, the location of the hot spots using coarser grids was not necessarily collocated with the location of the hot spots predicted with the finer grids, again introducing uncertainty into the risk assessments for "hot spot" assessments. .

V. SUMMARY

To improve the capability of Models-3 to simulating AQ at high resolution (~1 km horizontal grid spacing) for conditions in which significant urban morphological features must be considered, an UCP has been implemented inside MM5 following the drag-force approach to simulate meteorological fields inside the RSL. Grid-scale meteorology and chemistry simulations were performed for a modeling domain encompassing the Philadelphia, PA metropolitan area. These initial results clearly show that the UCP implementation to the standard version of MM5 made significant changes to the predicted meteorological fields at high resolution. The modification of the turbulent length scale parameterization under unstable conditions and the implementation of the UCP give encouraging results to give to MM5 the capability to be used at NS. It was found that

the turbulent length scale parameterization of Bougeault and Lacarrère (1989), when applied to the GSPBL, provided a method for dampening potentially spurious waves in the meteorological predictions. Comparison with and without the UCP shows that meteorological field differences above the canopy are stronger above and downwind of the city during the evening and the night. Simulation with the UCP exhibits an increase of the air temperature and of the MH, and a slight decrease of the wind speed. Inside the urban RSL, the mean vertical meteorological profiles with the UCP are improved in comparison to the case without the UCP. These results show that the UCP in MM5 simulates meteorological profiles similar to observations and to UCPs in other mesoscale models (e.g., M02 and Vu et al., 2002), but a more thorough evaluation of the UCP against measurements is required.

A limited set of pollutant concentration fields were examined including CO, NO_x, ozone, and formaldehyde and acetaldehyde. The major points of these simulations are as follows: (1) At NS, from the sensitivity studies, CMAQ demonstrated a strong sensitivity of pollutant concentration fields to the MM5 derived meteorological fields with and without UCP because of the increase of the MH during the evening and the night and because of the increase of the turbulent mixing in the RSL. Further, the simulations with UCP applied made large difference to the predicted concentrations, affecting both their magnitude and detail of their spatial distributions. Additional spatial structure to the concentration fields was resolved at NS primarily due to the finer structure of the source distribution field. There remains the question of additional spatial detail unresolved at 1.33 km resolution, the so-called SGV variability, a subject that will be discussed further in the next section.

Thus, by modeling at NS and by introducing a UCP, we demonstrate a capability for more realistic AQ simulations and at a scale for which important spatial features in the pollutant fields can be resolved. These implications allow for more accurate photochemical assessments as well as for addressing desired applications such as “hot spot” analyses. From preliminary results of these and other pollutants species, we observe that the extent of the resolved-scale spatial variability differ for different pollutant species and between urban and non-urban areas. The implication is that the grid resolution selected for use in exposure modeling may need to be ascertained by numerical experiments.

VI. FUTURE DIRECTIONS

In this section, we indicate two modeling research areas needed to fulfill the design concept of using AQ modeling for exposure and risk based studies. First, we see refinements that can be made to this UCP. Second, we address the need for modeling additional spatial variability at sub

grid scales and suggest methodologies that can be explored. Due to it's important role in this modeling paradigm for exposure assessments, we provide cursory details to outline the key considerations. Finally, while not discussed further, it will be necessary, of course, to evaluate both the predictions of the grid resolved and SGV concentration fields. Clearly, while available observations may provide insights, additional, more specialized data may be needed.

i. UCP refinements: For this study, we utilized a UCP to account for the finite size of the building in urban land use categories. A new study is now underway (Ching et al., 2002a and b) that will allow the further examination of sensitivity of meteorology and AQ fields to additions and refinements in our current UCPs for more realistic accounting of influence of the urban morphological structure (UMS) fields on the modeled meteorological fields. This exploratory effort will utilize gridded UCPs based upon high resolution description (data) on the building, street and vegetation (tree) canopies across the modeling domain. The thermodynamic part of the UCP will also be improved by adapting the urban soil model SM2-U (Dupont et al. 2002) to the drag-force approach. Recent technology including stereo photogrammetry and/or airborne lidar data provides the high-resolution 3-D digital building and tree data sets. Consequently, the meteorological modeling will be greatly advanced when using detailed gridded UMS parameters that are based on such measurements. Such data and UCPs are being developed for a follow-on modeling simulation for Houston TX. Also, since the dispersion of emissions sources in urban areas will be influenced by UMS, this important detail will need attention in AQ models for urban sources and, especially, this consideration can be explored the context of this database of actual building and vegetation information.

ii. Sub-grid variability (SGV): Concentration variability at sub-grid scales is a component of the overall NS modeling paradigm. We briefly indicate here, some of the major considerations involved and suggested approaches to guide the SGV methods development. A property of grid models is that the local, near-source concentration distributions due to dispersion of point, line, and area sources are not explicitly treated; rather, emissions from such sources are immediately dispersed throughout the grid volume. Thus, the detailed concentrations distribution in the near-source regions will not be modeled. Consequently, exposure assessments utilizing grid resolution fields may significantly underestimate potential levels of human exposures in grid areas containing significant numbers of sources, especially in the urban areas. Computational Fluid Dynamics (CFD) modeling can resolve these fine details, but with large computational requirements. The applications design problem is to seek a model resolution large enough for practical computations, to be inclusive of appropriate parameterization formulations at that scale for handling the important contributing atmospheric processes and, yet also provides a means for estimating the near-source concentration distributions. For practical considerations, the latter requirement is addressed by developing

concentration probability density functions (PDF) as a means to estimate the sub-grid scale concentration distributions.

Here, we recognize and propose methodologies for handling two contributing sources of SGV. These SGV sources include: (1) spatial distributions from the within grid dispersion of point, mobile and area emission sources and from (2) photochemistry due to direct coupling between turbulent motions and reactive pollutants when chemical reaction time scales are on the order of the turbulent eddy time scale.

Approaches to estimating the PDFs from both source dispersion and from chemical-turbulent interactions may vary from a highly parameterized zeroth order formulations to puff (or plume)-in-grid to more deterministic formulations. For the zeroth order approach, it could be assumed a similitude between the SGV to be proportional to the within-grid source distribution for handling primary source dispersion. The justification for this approach improves for the larger grid size simulations. For photochemistry, parameterizations developed from using such techniques as coupled large-eddy simulation photochemical model, e.g., LESchem, (Herwehe 2000) can be used to address sub-grid-scale variability for pollutants with different chemical reactivity rates and turbulent transport time scales. Using this modeling approach, the chemistry and turbulent transport fields are solved as a coupled system, which allows bi-directional feedback between the chemistry and dynamics during the simulation. Results (Ching et al., 2001) indicate a wide range of sub-grid chemical variability for different pollutant species (e.g., large variability for formaldehyde and acetaldehyde; relatively small variability for carbon monoxide) at the surface as well as aloft in the mixed layer due to the degree of photochemical reactivity in atmospheric mixtures and various trace species chemical lifetimes. This suggests parametric possibilities such as Damkoehler number scaling for the PDFs.

Finally, as part of methodologies that link these modeling of ambient concentration fields, to human exposure models, it will be useful to include the development of methods to assimilate central site monitoring data. Eventually, the development will be advanced to generating predictive as well as retrospective assessments of risk.

Acknowledgements. The first and second authors were supported by EPA Interagency Agreement with NOAA (DW13938634). The third and fourth authors were supported at the Atmospheric Modeling Division through UCAR Visiting Scientist Program appointments. The authors thank Dr. Michael Brown (Los Alamos National Laboratory) for valuable discussions regarding the implementation of the urban canopy parameterization in MM5. The authors are grateful to Dr. Richard Ellefsen (San Jose State University) for providing additional information and insight on the morphology study of

Philadelphia. The authors are grateful to Dr. Jerry Herwehe (Atmospheric Turbulence and Diffusion Division, NOAA ARL, Oak Ridge, Tennessee) for his insights and collaborative contributions on LESChem referred to in the discussion of SGV. The authors acknowledge colleagues Dr. Daewon Byun (now at University of Houston), Dr. Jonathan Pleim, Dr. Jeffrey Young, and Thomas Pierce who provided valuable consultation on applying CMAQ at neighborhood scales. The authors also acknowledge Ruen Tang, George Pouliot, and Lara Reynolds who provided assistance with completing the CMAQ simulations while on contract with DynCorp. The authors also thank Kenneth Schere and William Petersen for their technical support during thie study, and for their technical reviews of this manuscript.

Disclaimer. The information in this manuscript has been prepared under funding by the United States Environmental Protection Agency. It has been subjected to Agency review and approved for publication. Mention of trade names or commercial products does not constitute endorsement or recommendation for use.

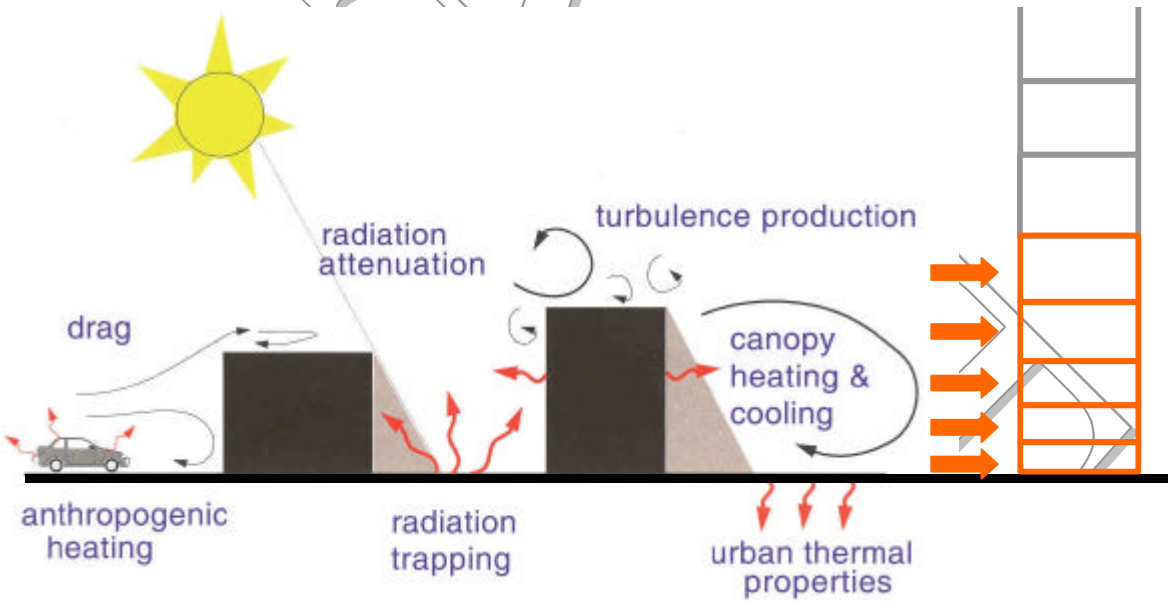

Figure 1: Urban canopy parameterization scheme (adapted from Dr. M. Brown, Los Alamos National Laboratory)

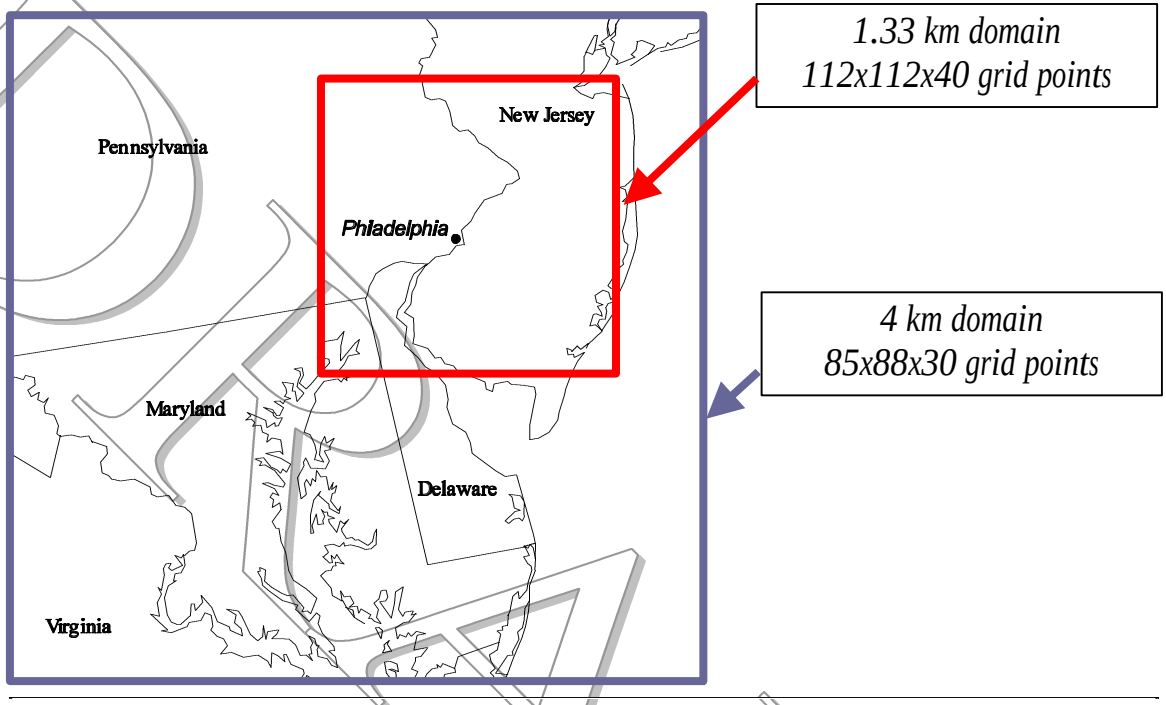

Figure 2: CMAQ modeling domain. The large domain applies is used for the 4 km grid mesh simulations; the smaller domain is for the simulation at 1.33 km grid size. The dot in the small domain is for central Philadelphia.

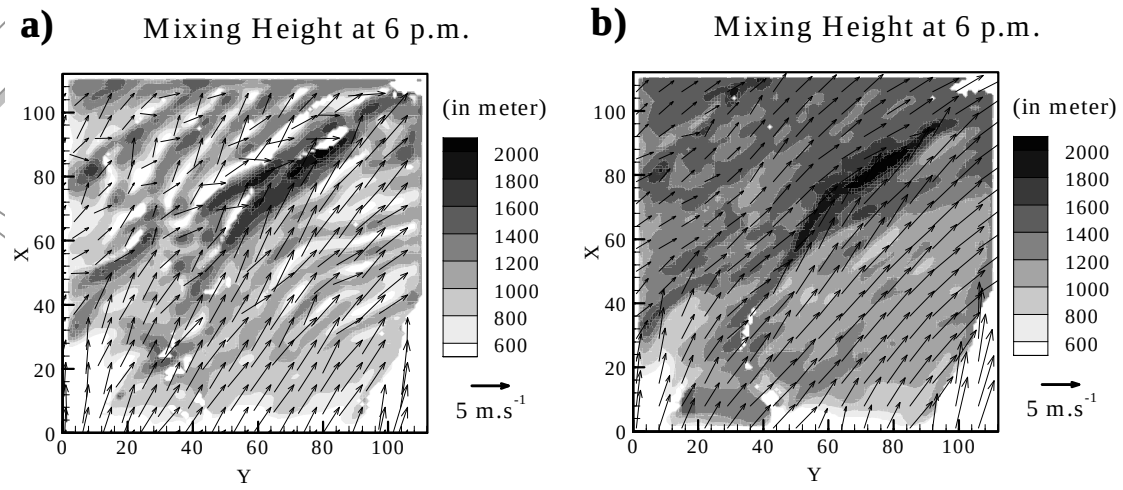

Figure 3: Comparison at 6 p.m. of the mixing height and wind vectors at 50 m above the ground given by the standard version of MM5 using GS PBL (a) and the modified version including the turbulent length scale parameterization of Bougeault and Lacarrère (1989) inside GS PBL for unstable conditions (b).

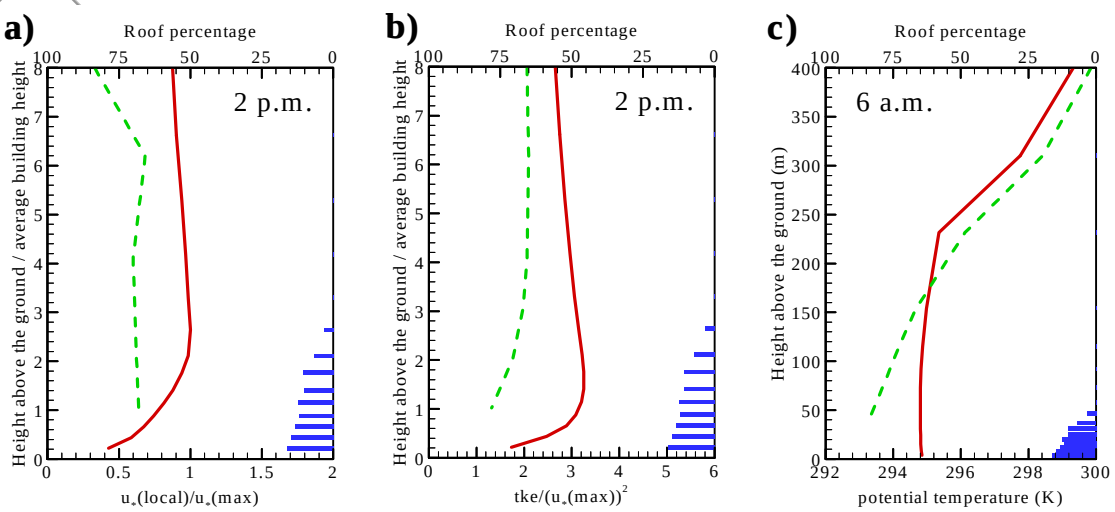

Figure 4: Vertical profiles at the city center of (a) the local u_* normalized by its maximum value at 2 p.m., (b) the ratio between tke and the maximum value of the local u_* at 2 p.m., and (c) of the air potential temperature at 6 a.m., for the cases with UCP (solid line) and without (dash line). The vertical roof percentage is indicated on the left side of the figures.

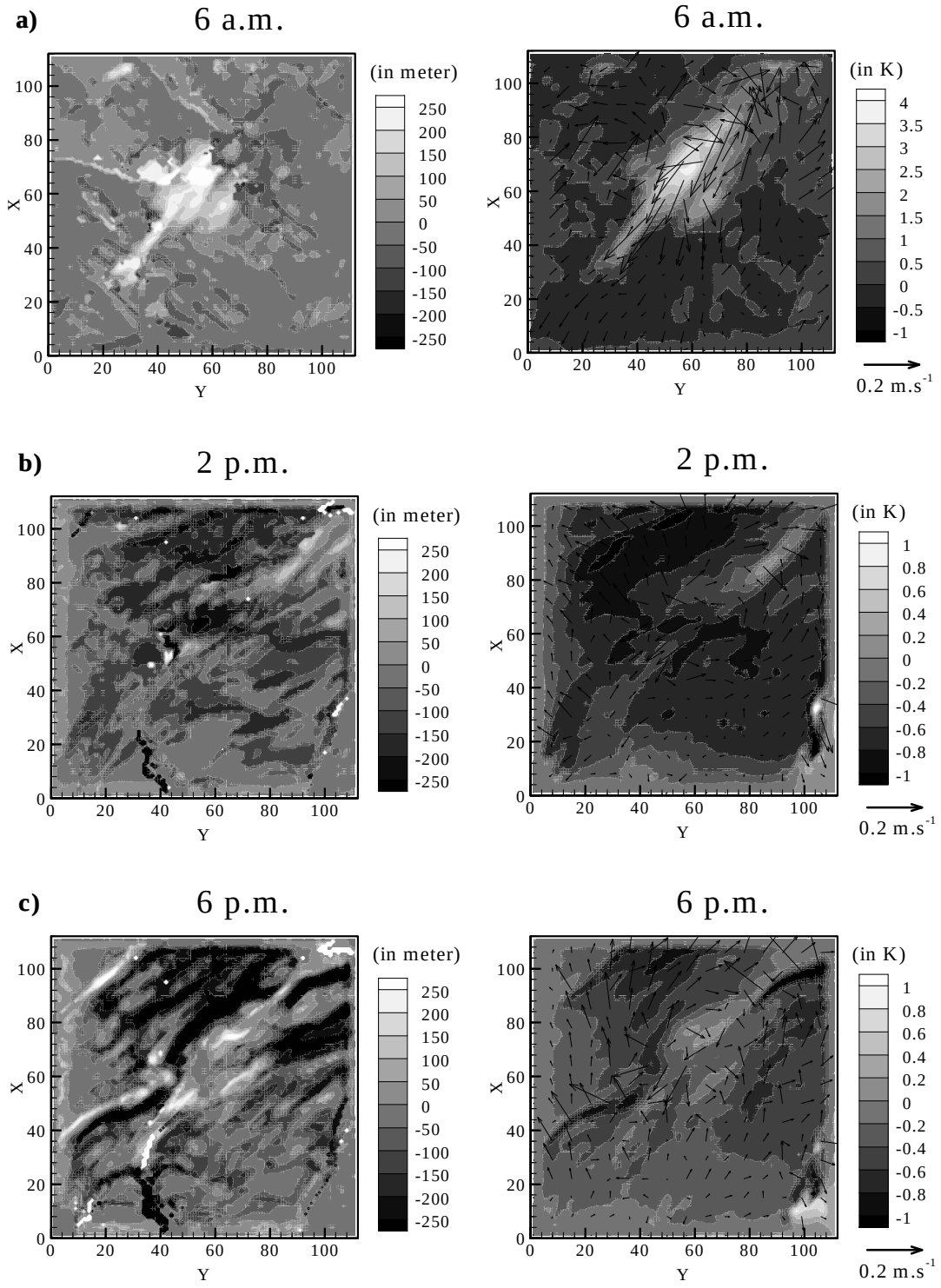

Figure 5: Difference fields of the mixing height (left figure), and air temperature and wind vectors at 50 m above the ground, between the case with the UCP and without, at 6 a.m. (a), 2 p.m. (b) and 6 p.m. (c).

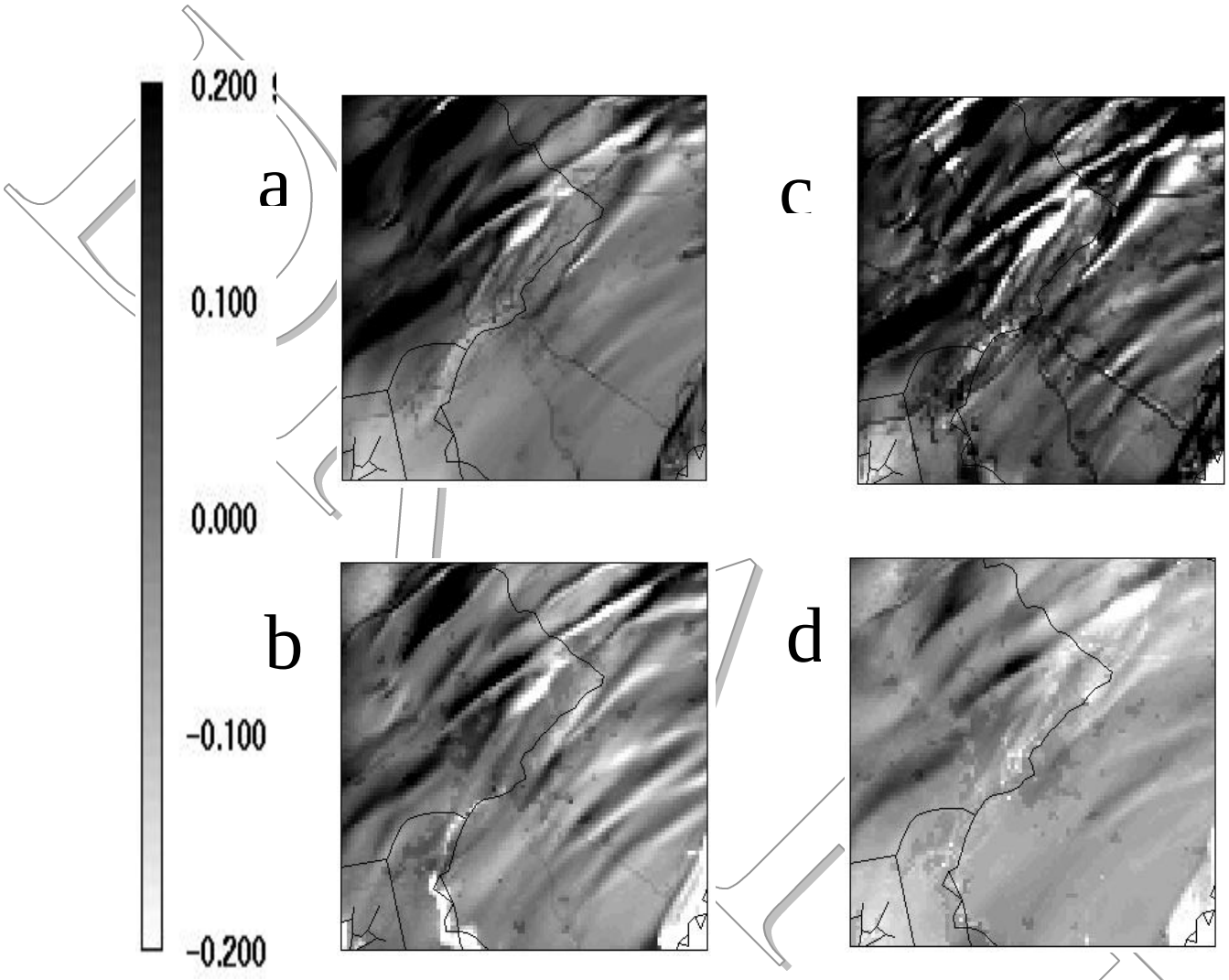

Figure 6a. CMAQ *nocam* simulations at 2 pm local time, July 14, 1995. Results are for the difference between layer 1 model outputs for runs with and without BL89 and normalized by the BL89 run for (a) CO, (b) formaldehyde, (c) NO_x, and (d) ozone.

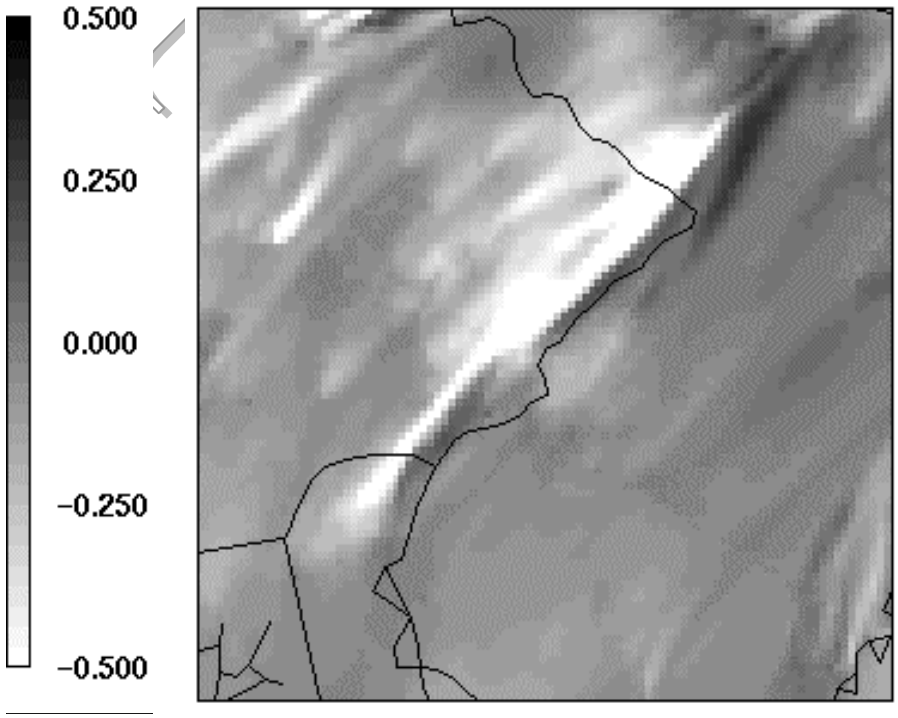

Figure 6b. Same as Figure 6a but only for CO at 6 pm EDT, July 14, 1995:

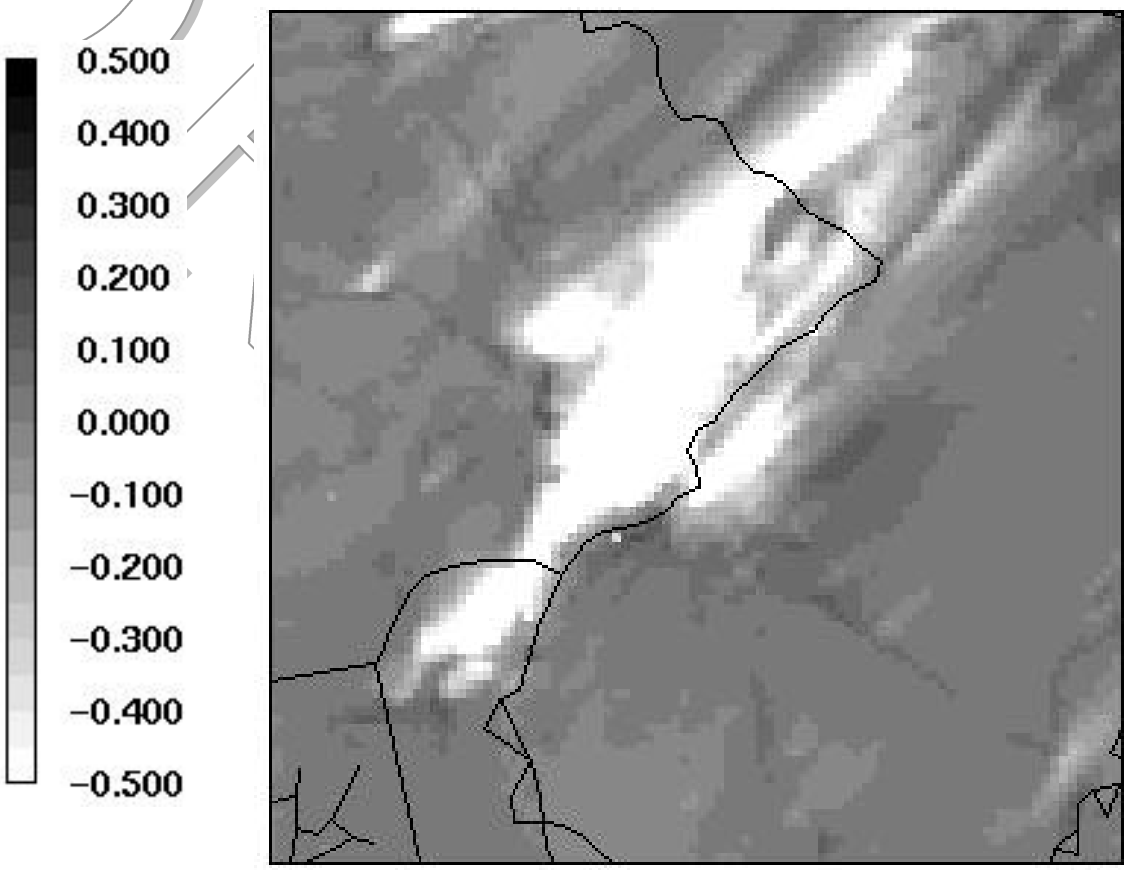

Figure 7. CMAQ simulation for CO at 6 am local time, July 14, 1995: Results are for the difference between layer 1 model outputs from runs with (*can*) and without UCP (*nocan*) and normalized by the run with UCP. These runs have BL89 applied.

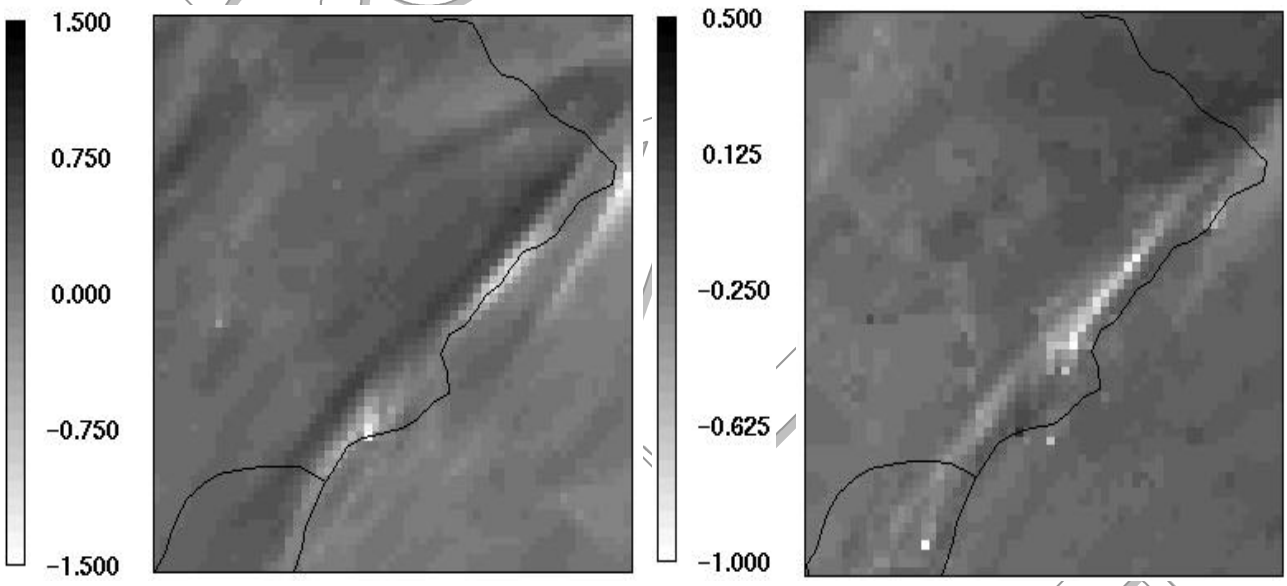

Figure 8. Normalized difference (same as Figure 7) but for NO (left)$_x$ and ozone (right) at 6 pm local time, July 14, 1995:

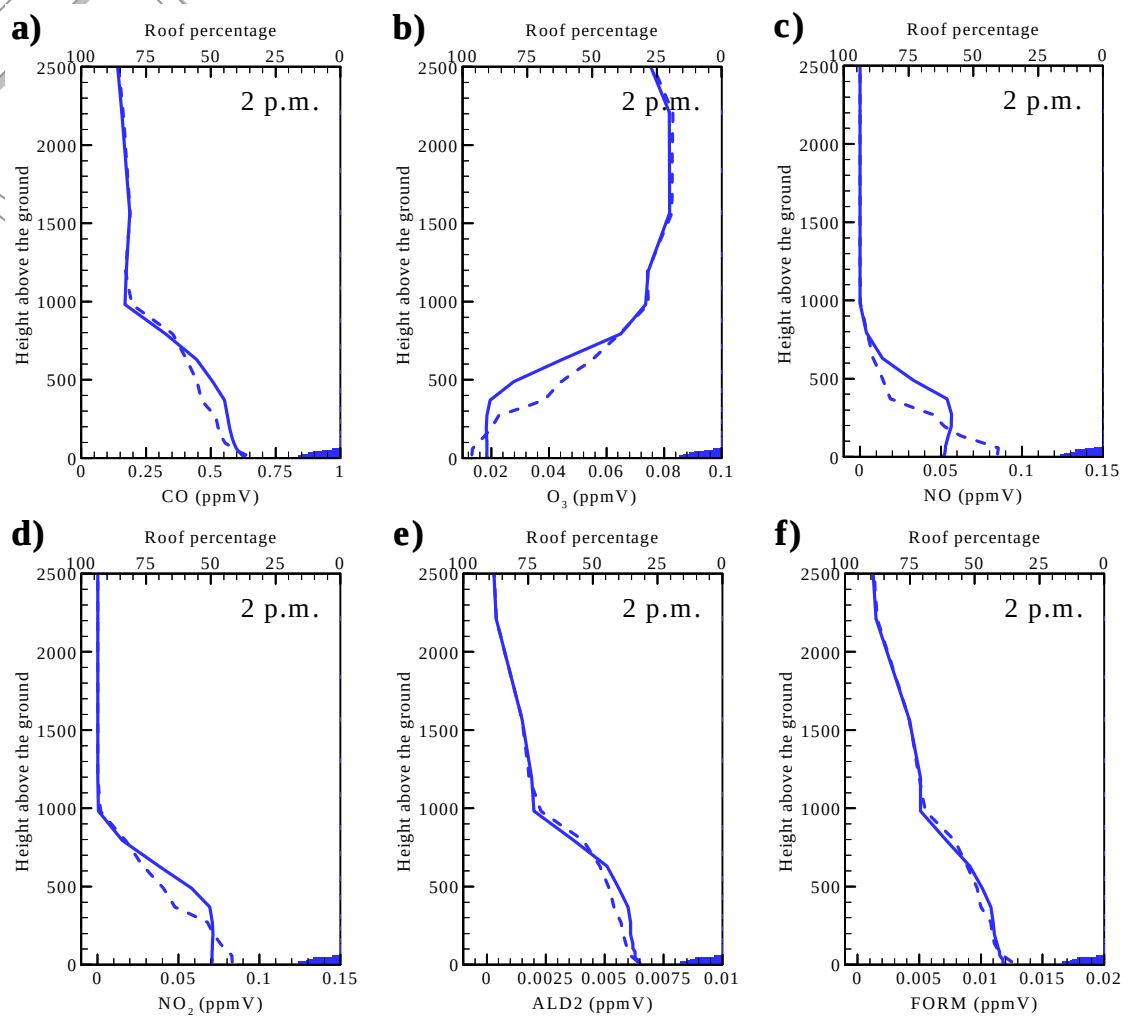

Figure 9: Vertical profiles at the city center of CO (a), O_3 (b), No (c), No_2 (d), Ald2 (e) and FORM (f) for the cases with UCP (solid line) and without (dash line). The vertical roof percentage is indicated on the left side of the figures.

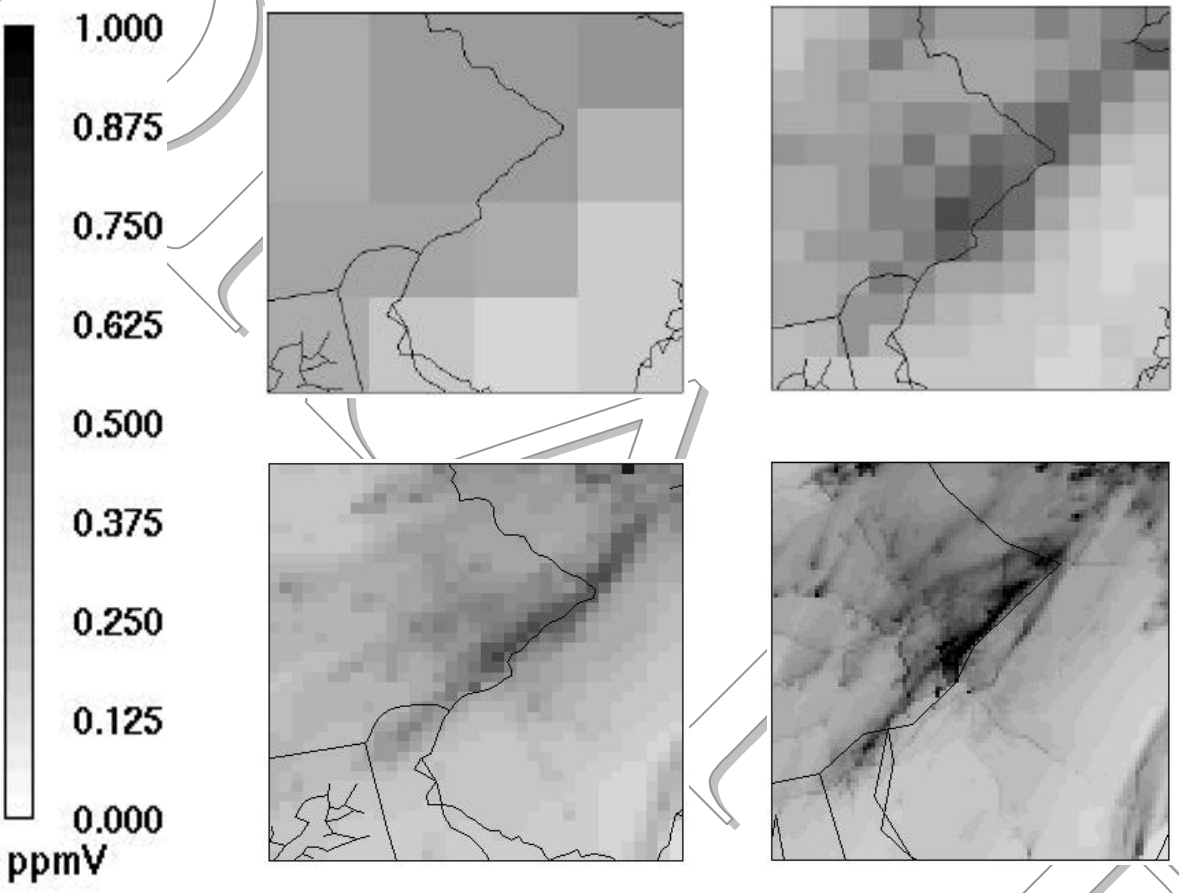

Figure 10. Results of CO from CMAQ for simulation time at 6 pm local time on July 14, 1995 for the 1.33 km grid domain. The simulation is for (a) 36 km, (b) 12 km, (c) 4 km runs are made without UCP applied. The results for (d) at 1.33 km resolution has UCP applied.

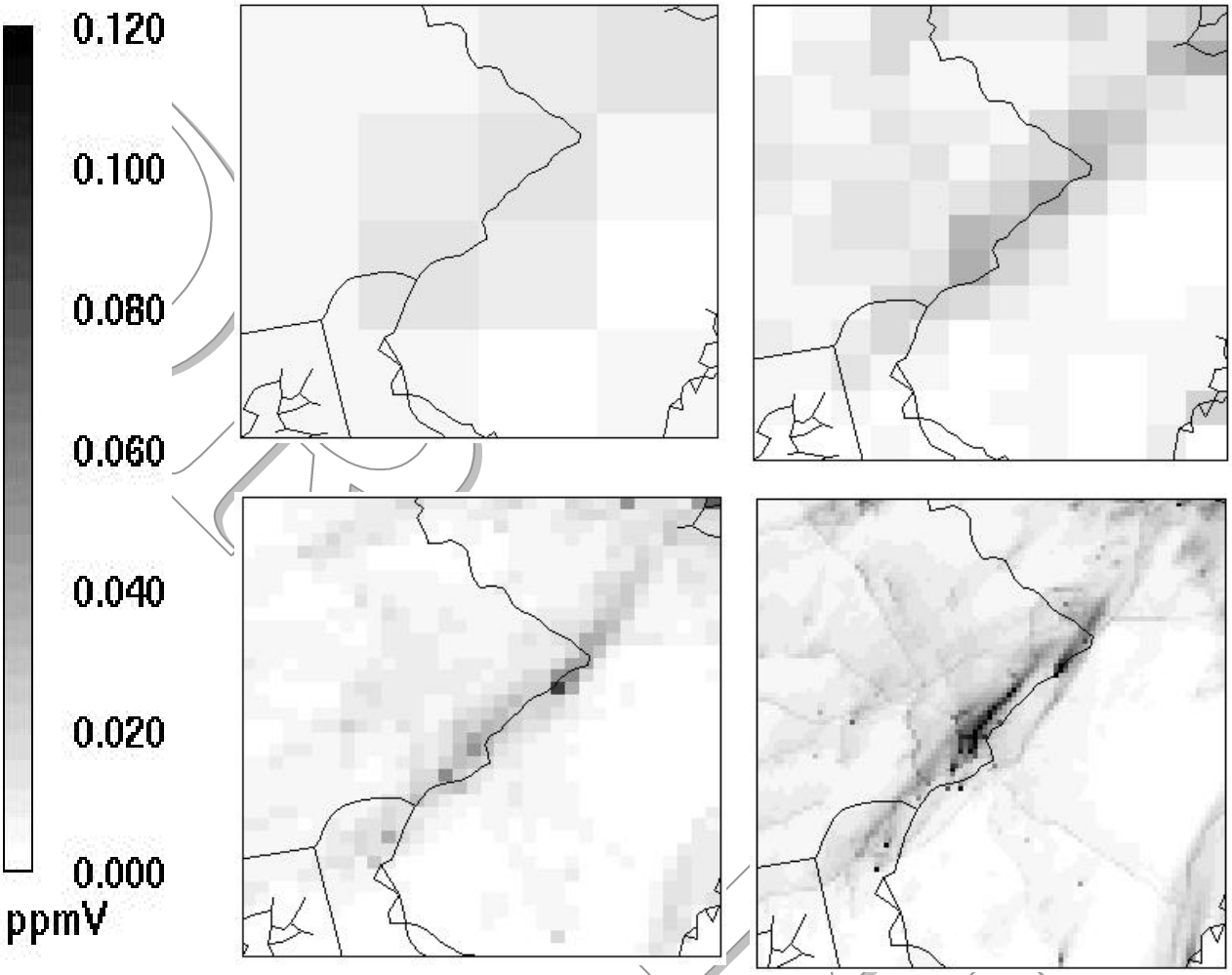

Figure 11. Same as in Figure 10 but for NO_x.

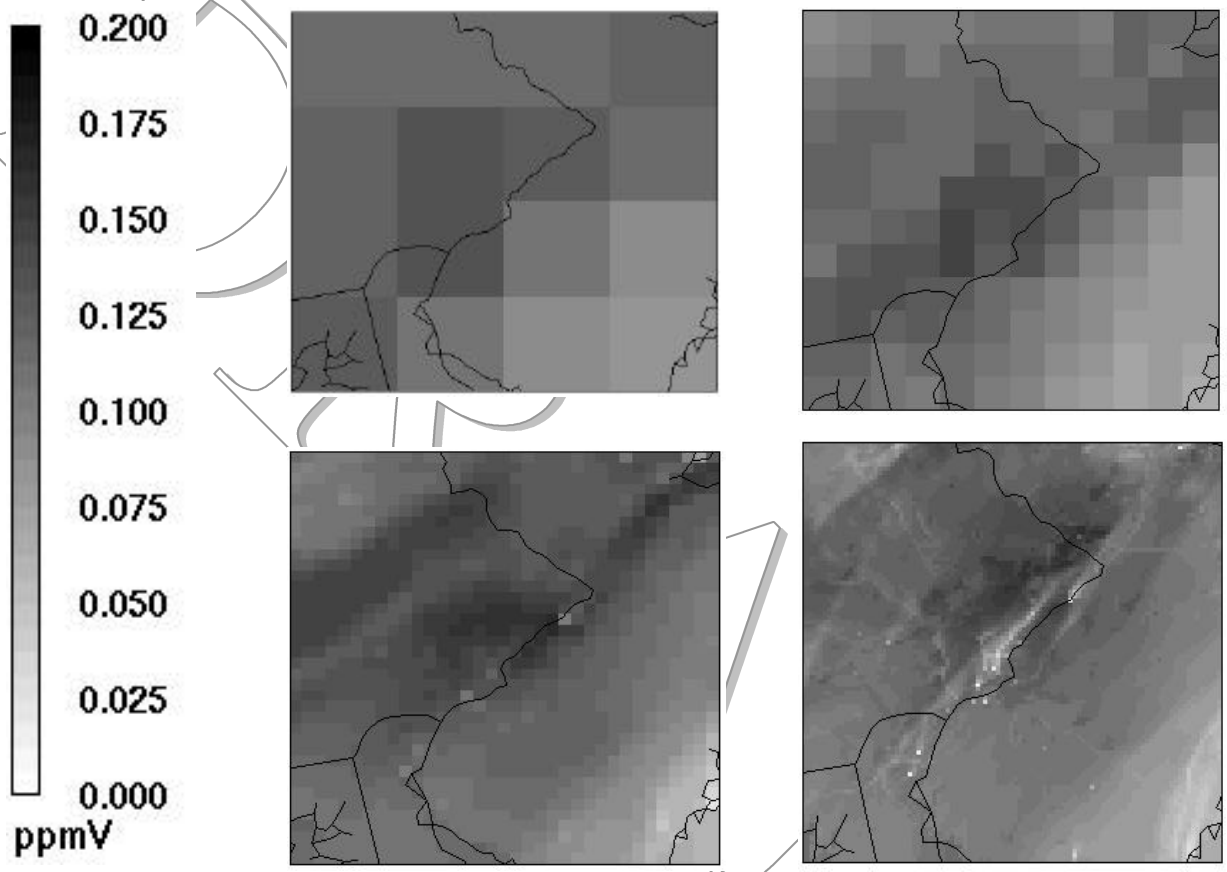

Figure 12. Same as in Figure 10 but for ozone.

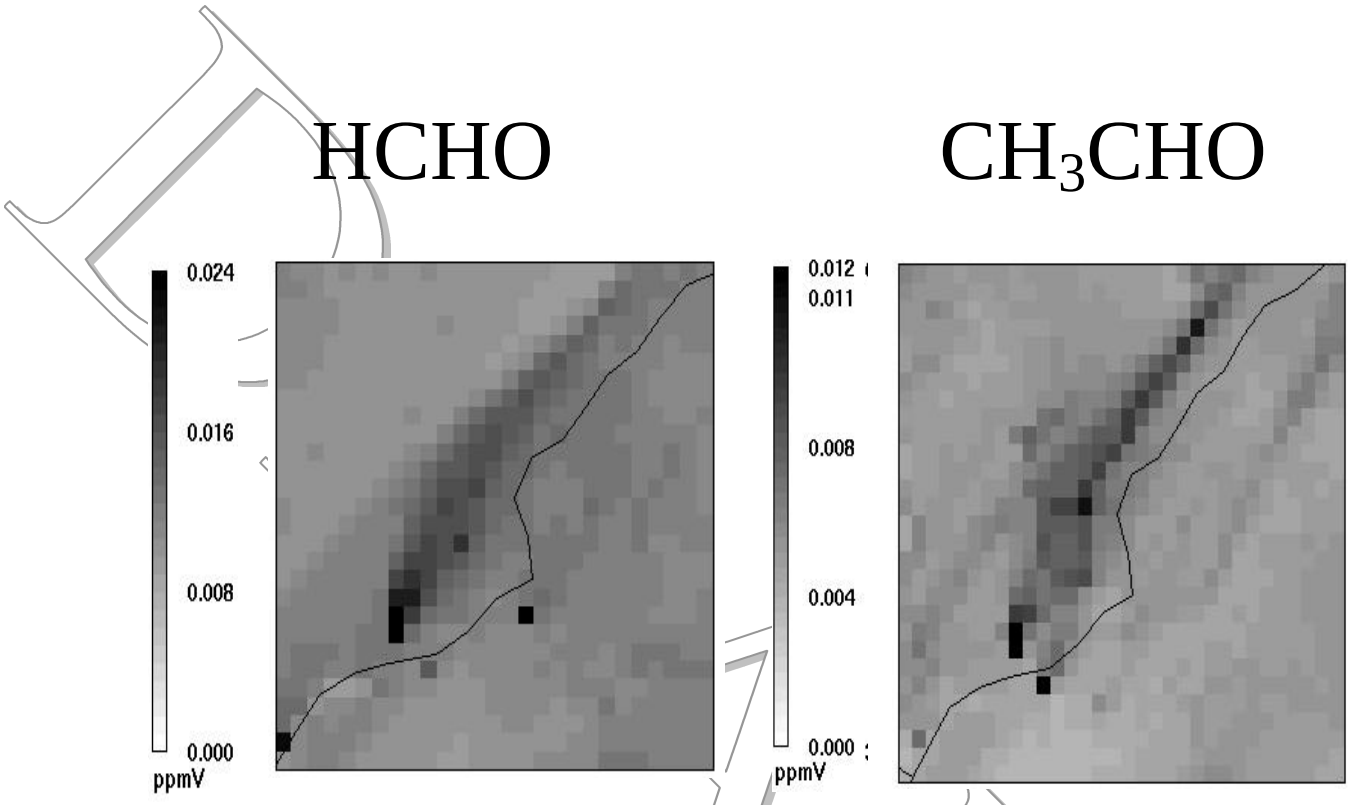

Figure 13. CMAQ (with UCP (*can*) applied) simulation of formaldehyde and acetaldehyde in layer 1 at 1.33 km resolution for 6 pm local time, July 14, 1995. The domain is for central Philadelphia covering a 40X40 km horizontal area.

VII. REFERENCES

Bélair, S., J. Mailhot, J. W. Strapp, and J. I. MacPherson, 1999: An examination of local versus nonlocal aspects of a TKE-based boundary layer scheme in clear convective conditions. *J. Appl. Meteor.*, **38**, 1499–1518.

Berman, S., J.-Y. Ku, and S. T. Rao, 1999: Spatial and temporal variation in the mixing depth over the northeastern United States during the summer of 1995. *J. Appl. Meteor.*, **38**, 1661–1673.

Binkowski, F. S., and U. Shankar, 1995: The regional particulate model. 1. Model description and preliminary results. *J. Geophys. Res.*, **100**, 26191–26209.

Bougeault, P., and P. Lacarrère, 1989: Parameterization of orography-induced turbulence in a mesobeta-scale model. *Mon. Wea. Rev.*, **117**, 1872–1890.

Brown, M. J., and M. D. Williams, 1998: An urban canopy parameterization for mesoscale models. Preprints, *Second Urban Env. Sym.*, Albuquerque, NM, Amer. Meteor. Soc., 144–147.

Brown, M. J, 2000: Urban parameterizations for mesoscale meteorological models. *Mesoscale Atmospheric Dispersion*, Z. Boybeyi (ed.) Wessex Press, 448 pp.

Burke, J. M., M. J. Zufall, and H. A. Ozkaynak, 2001: A population exposure model for particulate matter: case study results for PM2.5 in Philadelphia, PA. *Journal of Exposure Analysis and Environmental Epidemiology*, **11(6)**, 470–489.

Byun, D. W., and J. K. S. Ching, 1999: Science algorithms of the EPA Models-3 Community Multiscale Air Quality (CMAQ) Modeling System. EPA/600/R-99/030.

Chin, H. S., M. L. Leach, and M. J. Brown, 2000: A sensitivity study of the urban effect on a regional scale model: an idealized case. Preprints, *Third Sym. Urban Env.*, Davis, CA, Amer. Meteor. Soc., 76–77.

Ching, J., A. Lacser, T. L. Otte, D. Byun, and J. Herwehe, 2001: Modeling toxics and $PM_{2.5}$ concentration fields as a means for facilitating human exposure assessments. Proceedings, *10th International Sym. "Transport and Air Pollution"*, NATO, 17–24.

Ching, J., T. L. Otte, S. Dupont S Burian and A. Lacser, 2002a: Urban morphology for Houston to drive Models-3 /CMAQ at neighborhood scales. Preprints, *Fourth Sym. Urban Env.*, Norfolk, VA, Amer. Meteor. Soc., 35–36.

Ching, J., A. Lacser, T. L. Otte, J. Herwehe, and D. Byun, 2002b: Neighborhood scale modeling of $PM_{2.5}$ and air toxics concentration distributions to drive human exposure models. Preprints, *12th Joint AMS Conf. on Air Pollution Meteorology with the AWMA*, Amer. Meteor. Soc., Norfolk, VA, 97–98.

Christen, A., R. Vogt, M. W. Rotach, and E. Parlow, 2002: First results from BUBBLE I: profiles of fluxes in the urban roughness sublayer. Preprints, *Fourth Sym. Urban Env.* Norfolk, VA, Amer. Meteor. Soc., 105–106.

Colella, P., and P. R. Woodward, 1984: The piecewise parabolic method (PPM) for gas-dynamic simulations. *J. Comp. Phys.*, **54**, 174–201.

Dudhia, J. 1989: Numerical study of convection observed during the winter monsoon experiment using a mesoscale two-dimensional model. *J. Atmos. Sci.*, **46**, 3077–3107.

Dupont, S., I. Calmet, and P. Mestayer, 2002: Urban canopy modeling influences on urban boundary layer simulation. Preprints, *Fourth Sym. on the Urban Environment*, Amer. Meteor. Soc., Norfolk, VA.

Ellefsen, R., 1990-91: Mapping and measuring buildings in the canopy boundary layer in ten U.S. cities. *Energy and Buildings*, **15–16**, 1025–1049.

Feigenwinter, C., R. Vogt, and E. Parlow, 1999: Vertical structure of selected turbulence characteristics above an urban canopy. *Theor. Appl. Climatol.*, **62**, 51–63.

Gery, M. W., G. Z. Whitten, J. P. Killus, and M. C. Dodge, 1989: A photochemical kinetics

mechanism for urban and regional scale computer modeling. *J. Geophys. Res.*, **94**, 12925–12956.

Grell, G., J. Dudhia, and D. R. Stauffer, 1994: A description of the Fifth-Generation Penn State/NCAR Mesoscale Model (MM5). NCAR/TN-398+STR, 138 pp.

Grimmond, C. S. B., and T. R. Oke, 1999: Aerodynamic properties of urban areas derived from analysis of surface form. *J. Appl. Meteor.*, **38**, 1262–1292.

Hertel, O., R. Berkowicz, J. Christensen, and O. Hov, 1993: Test of two numerical schemes for use in atmospheric transport-chemistry models. *Atmos. Environ.*, **27A**, 2591–2611.

Herwehe J. A., 2000: A numerical study of the effects of large eddies on trace gas measurements and photochemistry in the convective boundary layer. Ph.D. Dissertation, Department of Atmospheric Sciences. University of Alabama in Huntsville. 242 pp.

Houyoux, M. R., J. M. Vukovich, C. J. Coats, Jr., N. W. Wheeler, and P. S. Kasibhatla, 2000: Emission inventory development and processing for the Seasonal Model for Regional Air Quality (SMRAQ) project. *J. Geophys. Res.*, **105**, 9079–9090.

Huang, H., and J. S. Chang, 2001: On the performance of numerical solvers for a chemistry submodel in three-dimensional air qualtiy models. 1. Box model simulations. *J. Geophys. Res.*, **106**, 20175–20188.

Kastner-Klein, P., M. W. Rotach, M. J. Brown, E. Fedorovich, and R. E. Lawson, 2000: Spatial variability of mean flow and turbulence fields in street canyons. Preprints, *Third Sym. Urban Env.* Davis, CA, Amer. Meteor. Soc., 13–14.

Kropfli, R. A., and N. M. Kohn, 1978: Persistent horizontal rolls in the urban mixed layer as revealed by dual-Doppler radar. *J. Appl. Meteor.*, **17**, 669–676.

Ku, J.-Y., H. Mao, K. Zhang, K. Civerolo, S. T. Rao, C. R. Philbrick, B. Doddridge, and R Clark, 2001: Numerical investigation of the effects of boundary -layer evolution on the predictions of ozone and the efficacy of emission control options in the northeastern United States. *Env. Fluid Mech.*, **1**, 209–233.

Lacser, A., and T. L. Otte, 2002: Implementation of an urban canopy parameterization in MM5. Preprints, *Fourth Sym. Urban Env.*, Norfolk, VA, Amer. Meteor. Soc., 153–154.

Martilli, A., A. Clappier, and M. W. Rotach, 2002: An urban surface exchange parameterisation for mesoscale models. *Bound-Layer Meteor.*, **104**, 261–304.

Mlawer, E. J., S. J. Taubman, P. D. Brown, M. J. Iacono, and S. A. Clough, 1997: Radiative transfer for inhomogeneous atmospheres: RRTM, a validated correlated-k model for the longwave. *J. Geophys. Res.*, **102 (D14)**, 16663–16682.

Oikawa, S., and Y. Meng, 1995: Turbulence characteristics and organised motions in a suburban roughness sublayer. *Bound.-Layer Meteor.*, **74**, 289–312.

Oke T. R., 1995: The heat island of the urban boundary layer: characteristics, causes and effects. In

J. E. Cermak et al. (eds), *Wind Climate in Cities*, Kluwer Academic Publishers, Dordrecht, Boston, pp. 81–107.

Otte, T. L., and A. Lacser. 2001: Implementation of an urban canopy parameterization in MM5 for meso-gamma-scale air quality modeling applications. Preprints, *Ninth Conf. on Mesoscale Processes*, Fort Lauderdale, FL, Amer. Meteor. Soc., 78–81.

Otte, T. L., and A. Lacser, 2002: Implementation of an urban canopy parameterization for fine-scale simulations. Preprints, *Twelfth PSU/NCAR Mesoscale Model Users' Workshop*, Boulder, CO, National Center for Atmospheric Research, 138–140.

Pielke, R. A., 1984: *Mesoscale Meteorological Modeling*. Academic Press, 612 pp.

Pielke, R. A., and M. Uliasz, 1998: Use of meteorological models as input to regional and mesoscale air quality models — limitations and strengths. *Atmos. Environ*., **32**, 1455–1466.

Pierce, T., C. Geron, L. Bender, R. Dennis, G. Tonnesen, and A. Guenther, 1998: Influence of increased isoprene emissions on regional ozone modeling. *J. Geophys. Res*., **103**, 25611–25629.

Pleim, J. E., and J. S. Chang, 1992: A non-local closure model for vertical mixing in the convective boundary layer. *Atmos. Environ.*, **26A**, 965–981.

Reisner, J., R. J. Rasmussen, and R. T. Bruintjes, 1998: Explicit forecasting of supercooled liquid water in winter storms using the MM5 mesoscale model. *Quart. J. Roy. Meteor. Soc*., **124B**, 1071–1107.

Rotach, M., 1995: Profiles of turbulence in and above an urban street canyon, *Atmos. Environ*., **29**,1473–1486.

Rotach, M. V., 2001: Urban scale dispersion modeling using a lagrangian particle dispersion model. *Bound.-Layer Meteor*., **99**, 379–410.

Roth M., 2000: Review of atmospheric turbulence over cities. *Quart. J. Roy. Meteor. Soc.*, **126**, 941–990.

Saeger, M., J. Langstaff, R. Walters, L. Modica, D. Zimmerman, D. Fratt, D. Dulleba, R. Ryan, J. Demmy, W. Tax, D. Sprague, D. Mudgett, and A. S. Warner, 1989: The 1985 NAPAP emissions inventory (Version 2): Development of the annual data and modelers' tapes. EPA-600/7-89-012a. 692 pp.

Seaman, N. L., 2000: Meteorological modeling for air-quality assessments. *Atmos. Environ*., **34**, 2231–2259.

Seaman, N. L., and S. A. Michelson, 2000: Mesoscale meteorological structure of a high-ozone episode during the 1995 NARSTO-Northeast study. *J. Appl. Meteor*., **39**, 412–426.

Shafran, P. C., N. L. Seaman, and G. A. Gayno, 2000: Evaluation of numerical predictions of boundary layer structure during the Lake Michigan Ozone Study. *J. Appl. Meteor*., **39**, 412–426.

Stauffer, D. R., and N. L. Seaman, 1994: Multiscale four-dimensional data assimilation. *J. Appl. Meteor.*, **33**, 416–434.

Taha, H., 1999: Modifying a mesoscale model to better incorporate urban heat storage: A bulk parameterization approach. *J. Appl. Meteor.*, **38**, 466–473.

Vu, T. C., Y. Ashie, and T. Asaeda, 2002: A k- turbulence closure model for the atmospheric boundary layer including urban canopy. *Bound.-Layer Meteor.*, **102**, 459–490.

Wesely, M. L., 1989: Parameterization of surface resistances to gaseous dry deposition in regional-scale numerical models. *Atmos. Environ.*, **23**, 1293–1304.

Yamada, T., 1982: A numerical model study of turbulent airflow in and above a forest canopy. *J. Met. Soc. Japan*, **60 (1)**, 439–454.

Zhang, D.-L., and R. A. Anthes, 1982: A high-resolution model of the planetary boundary layer — Sensitivity tests and comparisons with SESAME-79 data. *J. Appl. Meteor.*, **21**, 1594–1609.

Zhang, K., H. Mao, K. Civerolo, S. Berman, J.-Y. Ku, S. T. Rao, B. Doddridge, C. R. Philbrick, and R. Clark, 2001: Numerical investigation of boundary-layer evolution and nocturnal low-level jets: local versus non-local PBL schemes. *Env. Fluid Mech.*, **1**, 171–208.

FIGURE CAPTIONS

Figure 1: Urban canopy parameterization scheme (adapted from Dr. M. Brown, Los Alamos National Laboratory)

Figure 2: Modeling domains Large domain for the 4 km grid mesh simulations; the smaller domain for the simulation at 1.33 km grid size. The middle point corresponds to where vertical profiles are studied.

Figure 3: Comparison at 6 p.m. (LDT) of the mixing height and wind vectors at 50 m above the ground given by the standard version of MM5 using GS PBL (a) and the modified version including the turbulent length scale parameterization of Bougeault and Lacarrère (1989) inside GS PBL for unstable conditions (b). Vertical and horizontal axes correspond to the grid number of the MM5 domain.

Figure 4: Vertical profiles at the city center of (a) the local u_* normalized by its maximum value at 2 p.m., (b) the ratio between TKE and the maximum value of the local u_* at 2 p.m. (LDT), and (c) of the air potential temperature at 6 a.m., for the cases with UCP (solid line) and without (dash line). The vertical roof percentage is indicated on the left side of the figures.

Figure 5: Difference fields of the mixing height (left figure), and air temperature and wind vectors at 50 m above the ground, between the case with the UCP and without, at 6 a.m. (LDT) (a), 2 p.m. (b) and 6 p.m. (c). Vertical and horizontal axes correspond to the grid number of the MM5 domain.

Figure 6: CMAQ simulation for CO at 6 pm local time, July 14, 1995: Results are for the difference between layer 1 model outputs from runs with and without BL89 and normalized by the run with BL89. These runs do not have UCP (*nocam*) applied.

Figure 7: CMAQ simulation for CO at 6 am local time, July 14, 1995: Results are for the difference between layer 1 model outputs from runs with (*can*) and without UCP (*nocan*) and normalized by the run with UCP. These runs have BL89 applied.

Figure 8: Normalized difference (same as Figure 7) but for NO_x and ozone at 6 pm local time, July 14, 1995:

Figure 9: Vertical profiles of selected pollutants from CMAQ run at 1.33 km (July 14, 1995) with UCP (*can*), solid line, and without UCP (*nocan*), dashed line, for a site in central Philadelphia. The vertical roof percentage is indicated on the left side of the figures..

Figure 10: CO from CMAQ for simulation time at 6 pm local time on July 14, 1995 for the domain of the 1.33 km grid. The simulation is for (a) 36 km, (b) 12 km, (c) 4 km runs made without UCP applied. The results for (d) at 1.33 km resolution has UCP applied.

Figure 11: Same as in Figure 10 but for $NO_{x.}$

Figure 12: Same as in Figure 10 but for ozone.

Figure 13: CMAQ (with UCP (*can*) applied) layer 1 simulation of formaldehyde and acetaldehyde at 1.33 km resolution at 6 pm local time, July 14, 1995. The domain is for central Philadelphia covering a 40X40 km horizontal area.